Proceedings of the ASME 2010 3rd Joint US-European Fluids Engineering Summer Meeting and 8th International Conference on Nanochannels, Microchannels, and Minichannels
FEDSM-ICNMM2010
August 1-5, 2010, Montreal, Canada

FEDSM-ICNMM2010-31165

PARAMETRIC STUDY OF A TRANSIENT LIQUID FLOW IN A MICROCHANNEL OF SQUARE CROSS-SECTION

Guyh Dituba Ngoma
University of Quebec in Abitibi-Temiscamingue
Department of Applied Sciences
445, Boulevard de l'Université
Rouyn-Noranda, Quebec, J9X 5E4, Canada

Amsini Sadiki
Darmstadt University of Technology
Department of Energy and Power Plant Technology
Petersenstrasse 30, 64287 Darmstadt, Germany

ABSTRACT

Time-dependent laminar liquid flow and thermal characteristics in a square cross-section microchannel were numerically investigated using computational fluid dynamics code. In the numerical model developed the upper and bottom microchannel substrate properties, Joule heating caused by applying electric potential, pressure driven flow, electroosmosis, heat transfer coefficients on the microchannel bottom wall and variations in the liquid thermophysical properties were all taken into account. Liquid flow velocity distribution and temperature fields were calculated by solving both Navier-Stokes and energy equations, and electric field distribution was determined based on their electric potential. The results obtained demonstrate the impact that applied potential, pressure difference, heat transfer coefficient and microchannel dimensions have on liquid flow and thermal behaviors in a square microchannel. Finally, the results with the model developed were then compared with those of a liquid having constant thermophysical properties.

KEY WORDS

Microfluidics, Electroosmosis, Heat transfer, Modeling and Simulation.

NOMENCLATURE

A	Area (m^2)
b	width (m)
c_p	specific heat ($Jkg^{-1}K^{-1}$)
e	elementary charge (C)
E	external electric field strength (Vm^{-1})
h	height (m)
h_c	heat transfer coefficient ($Wm^{-2}K^{-1}$)
k	thermal conductivity ($Wm^{-1}K^{-1}$)
k_b	Boltzmann constant (JK^{-1})
L	microchannel length (m)
n_∞	ionic number concentration in the solution (m^{-3})
p	pressure (Pa)
Q	volumetric flow rate (ms^{-3})
q	heat flux (Wm^{-2})
T	temperature (K)
t	time (s)
u	liquid flow velocity in x-direction (ms^{-1})
v	liquid flow velocity in y-direction (ms^{-1})
w	liquid flow velocity in z-direction (ms^{-1})
x	x-axis coordinate (m)
y	y-axis coordinate (m)
z	z-axis coordinate (m)
z_e	valence of ions

Greek

Δ	difference
ε	dimensionless relative dielectric constant
ε_0	permittivity of vacuum ($Cm^{-1}\ V^{-1}$)
Φ	total electric potential (V)
ϕ	electric potential (V)
μ	dynamic viscosity (Pa s)
ρ	liquid density ($kg\ m^{-3}$)
σ	electric conductivity ($\Omega^{-1}m^{-1}$)
ψ	internal electric potential of the EDL (V)
ζ	zeta potential (V)

Subscripts

c cross-section
i inlet
L liquid
m mean value
o outlet
s solid
w wall

INTRODUCTION

Fluid transport in microfluidic devices plays an increasing role in the fields of biomechanical processes, biotechnologies, micropower generation, chemical processes, etc., where surface effects dominate flow behavior within electronic microdevices such as micropumps, microvalves, micromixers, microreactors, microflow sensors and microchannel heat sinks. The electric double layer (EDL) plays an important role in liquids transported by electroosmosis, particularly when a polar liquid comes into contact with a solid. The electric double layer thickness depends in part on ionic bulk concentrations and electric fluid properties found in a microchannel. To provide efficient control and ensure the reliability of microfluidic devices used to move fluids, accurate and detailed knowledge of liquid flows and thermal behavior in microchannels, for both initial and boundary conditions at liquid–solid interfaces, at both the microchannel inlet and outlet, and the microchannel wall must be taken into account [1,2]. Hence, in order to avoid critical operating conditions in microfluidic devices, liquid flow and thermal investigations related to various characteristics must be considered during the planning, design and optimization phases of microfluidic devices. Most previous investigations of the effects caused by pressure gradients, electroosmosis and heat transfer on liquid flows in microchannels were performed when considering a steady state [3,4]. Moreover, certain previously performed numerical studies only considered liquid flows in a three-dimensional microchannel in an unsteady-state, where electric potential was applied without any consideration being given to heat transfer [5-8]. Moreover, an analysis of previous work reveals that the results were specific to microchannel configurations and therefore could not be extrapolated to other configurations. In this work, the transient behavior of liquid flow is numerically investigated in order to gain further insight into the characteristics of pressure-driven flow, electroosmosis and heat transfer for a square cross-section microchannel, while taking their liquid temperature-dependent thermophysical properties and taking into account the microchannel materials. Liquid conductive media equations, time-dependent liquid flow Navier-Stokes equations and time-dependent energy equations in liquid and microchannel substrates are used to obtain a system of partial differential equations. This system is then numerically solved to determine electric field strength, liquid flow velocity and temperature distribution, respectively. Since EDL thickness is often in the order of nanometers, slip velocity approximation is introduced in order to neglect the thin EDL region, such that the entire flow is driven by the hydrodynamic shear stresses originating from the liquid's viscosity. This slip velocity is determined using the Smoluchowski equation, and hence in the final equations boundary conditions for wall zeta potential, Helmholtz-Smoluchowski electroosmotic velocity and wall heat transfer coefficients are taken into account. Based on the partial differential equations found, COMSOL Multiphysics 3.5a computational fluid dynamics code [9] is used to solve these equations and to analyze the effects caused by pressure difference, heat flux and microchannel dimensions on time-dependent liquid flow and on the thermal characteristics of the three-dimensional microchannel in the square cross-section.

MATHEMATICAL FORMULATION

Fig. 1 shows the square microchannel model selected, consisting of an upper and bottom substrate. A heat transfer coefficient is imposed on the microchannel bottom, where constant zeta potentials are applied to the four microchannel inner walls, which are electrically non-conducting, and where the microchannel inlet and outlet are connected to two reservoirs with electric potentials ϕ_i and ϕ_o, respectively.

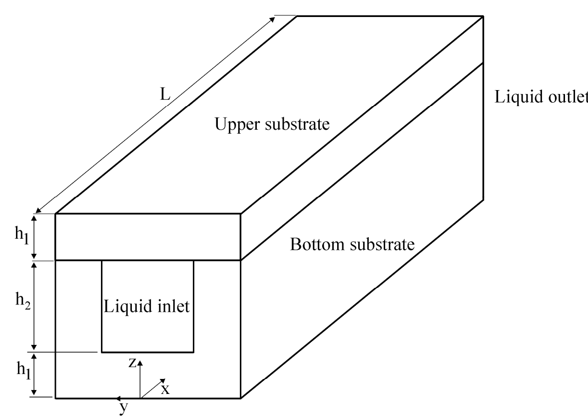

Figure 1: Microchannel of square cross-section

The following assumptions were made for the mathematical formulation: (i) unsteady-state, three-dimensional and laminar flow; (ii) fluid was incompressible. (iii) fluid was Newtonian. (iv) liquid thermophysical properties were temperature-dependent, except for the liquid specific heat; (v) substrate thermophysical properties were constant; (vi) symmetric electrolyte solution; (vii) zeta potential was uniform throughout the microchannel inner walls; (viii) electric double layer thickness, $\lambda_{EDL} = \sqrt{\frac{\varepsilon\varepsilon_0 k_b T}{2n_\infty z_0^2 e^2}}$ was much smaller than microchannel dimensions, and thus the electroosmotic flow (EOF) velocity was used as a boundary velocity.

To account for these assumptions, the theoretical analyses for pressure driven flow, electroosmosis and thermal characteristics in a three-dimensional microchannel, as shown in Fig. 1, were based on equations giving steady electric conductive media, time-dependent Navier-Stokes and time-dependent heat transfer through convection and conduction.

Electric Potential Field

The liquid motion was initiated by the electrical body force acting on the ions in the EDL, where the electroosmotic flow was dependent on the applied electric field and the net electric charge in the liquid. The electric field was composed of two terms: the first being the electric field caused by the external applied electric potential for which the governing equation is

$$\nabla^2\phi = 0\,, \tag{1}$$

in the case of constant electric conductivity and the second being the electric field caused by the induced electric potential of the ions in EDL, expressed by

$$\nabla^2\psi = -\frac{\rho_e}{\varepsilon\varepsilon_0}\,, \tag{2}$$

where ε represents the solution's relative dielectric constant, ε_0 the vacuum permittivity, and ρ_e the net charge density.

The total electric potential can be formulated as $\Phi = \psi + \phi$ and the external applied electric field defined as

$$\vec{E} = -\nabla\phi\,. \tag{3}$$

ρ_e is related to ψ and is expressed in terms of the Boltzmann distribution as follows

$$\rho_e = -2n_\infty z_e e \sinh\left(\frac{z_e e}{k_B T_0}\psi\right), \tag{4}$$

where e, k_B, n_∞, T_0 and z_e represent elementary charge, Boltzmann constant, bulk ion concentration, ambient temperature and ion valence, respectively.

Velocity Profile

For a three-dimensional laminar Newtonian liquid flow through a square microchannel, as shown in Fig. 1, the working liquid's incompressibility is expressed by the continuity equation

$$\nabla.\vec{U} = 0\,, \tag{5}$$

and the Navier–Stokes equations are given by

$$\rho_L(T)\left(\frac{\partial\vec{U}}{\partial t} + \left(\vec{U}.\nabla\vec{U}\right)\right) = -\nabla p + \mu_L(T)\nabla^2\vec{U} + \rho_e\vec{E}\,, \tag{6}$$

where $\vec{U} = \vec{U}(u(x,y,z,t), v(x,y,z,t), w(x,y,z,t))$ is the liquid flow velocity vector, p is the pressure, T is the temperature, $\vec{E} = \vec{E}(E_x, E_y, E_z)$ is the external applied electric field vector, $\rho_L(T)$ is the temperature-dependent density, and $\mu_L(T)$ is the temperature-dependent dynamic viscosity.

The other symbols, subscripts, and superscripts used are defined in the nomenclature.

Since the net electric charge ρ_e formed by the EDL is zero, except in the thin EDL region adjacent to the microchannel wall and the microchannel dimensions are assumed to be much greater than the EDL thickness, the electrical force term in Eq. 6 can be dropped and the Helmholtz-Smoluchowski electroosmotic velocity, $\vec{U}_{hs} = -\frac{\varepsilon(T)\varepsilon_0\zeta\vec{E}}{\mu_L(T)}$, is used as a slip boundary condition on the microchannel wall for the Navier-Stokes equations, which becomes

$$\rho_L(T)\left(\frac{\partial\vec{U}}{\partial t} + \left(\vec{U}.\nabla\vec{U}\right)\right) = -\nabla p + \mu_L(T)\nabla^2\vec{U}\,. \tag{7}$$

For the initial conditions at $t_0 = 0$ Eq. 7 can be written for the liquid flow velocity as $\vec{U}(x,y,z,t_0) = 0$ and for the pressure as $p(x,y,z,t_0) = 0$.

As for the boundary conditions at the microchannel inlet and outlet, "pressure, no viscous stress boundary conditions" [9] are used according to $\mu_L(T)\left(\nabla\vec{U} + \left(\nabla\vec{U}\right)^T\right).\vec{n} = 0$ and $p = p_0$, where p_0 is the applied pressure and $\vec{n}$ is the normal vector, pointing outward from the domain being considered.

Using the liquid flow velocity vector, the volumetric flow rate can be obtained by integrating the flow velocity over the microchannel cross-section area as follows: $Q = \int_{A_c}\left(\vec{n}.\vec{U}\right)dA_c$.

Temperature Field

To account for the flow velocity field and the electric field, the time-dependent energy equations were used to obtain the temperature distribution within the liquid contained in the microchannel. Under the simplified assumptions of constant specific heat and constant electric conductivity, and neglecting the thermal energy generated in the microchannel due to viscous dissipation, the equations for the energy transport can be written as follows

$$\rho_L(T)c_{pL}\left(\frac{\partial T}{\partial t}+\vec{U}.\nabla T\right)=\nabla.(k_L(T)\nabla T)+\sigma_L(\vec{E}.\vec{E}), \quad (8)$$

where for this liquid c_{pL}, k_L and σ_L represent specific heat, thermal conductivity and electric conductivity, respectively.

For the microchannel substrate walls, the time-dependent energy equations can be given by

$$\rho_s c_{ps}\frac{\partial T_s}{\partial t}=\nabla.(k_s\nabla T_s). \quad (9)$$

Eqs. 8 and 9 are subject to the initial condition $T(x,y,z,t_0)=T_0$. For the liquid boundary conditions at the microchannel inlet, $T(x,y,z,t)=T_i$ and at the microchannel outlet $\vec{n}.(-k(T)\nabla T)=0$. For the microchannel substrates, the thermal insulation boundary conditions are applied according to $-\vec{n}(-k(T)\nabla T)=0$ on the substrate outer walls, except for the bottom wall of the bottom substrate, where a heat flux is formulated using the expression $-\vec{n}.(-k(T)\nabla T)=q$, where $q=h_c(T-T_0)$.

The differential partial equations found in this section were solved numerically using COMSOL Multiphysics 3.5a computational fluid dynamics code [9]. Based on the finite element method, this code is used to determine electric field, velocity distribution and temperature distribution in liquid flows and in microchannel substrates. For Eq. 7, the predefined 2nd order Lagrange p_2-p_1 elements were used to stabilize the pressure, where u, v, w, and p are the 2nd order piecewise polynomial used in the finite element space. For the convection and conduction modes, and for the conductive media, the predefined 2nd order Lagrange-Quadratic elements were used with T and ϕ respectively, the 2nd order piecewise polynomials in the finite element space [9]. Since k_L, ε, μ_L and ρ_L are temperature-dependent, Eqs. 7-9 form a coupled system that can be solved simultaneously, after Eq. 1 has been solved separately.

RESULTS AND DISCUSSION

Assuming that a dilute symmetrical electrolyte solution was considered as a working liquid having the same properties as water, in addition to being used as a basis the data below, was applied to carry out simulations for: $h_1 = 90 \times 10^{-6}$ m, $h_2 = 80 \times 10^{-6}$ m, L = 0.02 m, e = 1.6021×10^{-19} C, $n_\infty = 6.022 \times 10^{20}$ m^{-3}, $\varepsilon_0 = 8.854 \times 10^{-12}$ $Cm^{-1} V^{-1}$, ε =305.7exp(-T/219), z_e = 1, $K_B = 1.3805 \times 10^{-23}$ JK^{-1}, ϕ_i = 550 V, ϕ_o = 0 V, σ_L = 0.21 $\Omega^{-1}m^{-1}$, p_i = 0 kPa, h_c = 10 $Wm^{-2}K^{-1}$, c_{pL} = 4200 $Jm^{-1}K^{-1}$ and T_0 = 298 K.

The water temperature-dependent expressions for density, dynamic viscosity and thermal conductivity were used in the calculations in accordance with the materials library described in [9]. The data for the microchannel substrates are shown in Tab. 1.

Table 1: Pyrex Glass and Silicon [10]

	c_{ps} $Jkg^{-1}K^{-1}$	k_s $Wm^{-1}K^{-1}$	ρ_s kgm^{-3}
Pyrex glass: upper substrate	835	1.4	2225
Silicon: bottom substrate	712	148	2330

Effect of Applied Electric Potential on Liquid Flow Velocity and Temperature

To analyze the effect of the electric potential on the liquid flow velocity and the liquid temperature, the outlet applied electric potential was kept constant at 0 V. The inlet applied electric potentials of 100 V, 250 V, 400 V and 550 V were then selected and Fig. 2 shows, at the steady-state, the resulting x-component liquid flow velocity distribution along the center line in the z-direction at the microchannel outlet. It can thus be seen that the liquid flow velocity increased when the applied electric potential at the inlet increased.

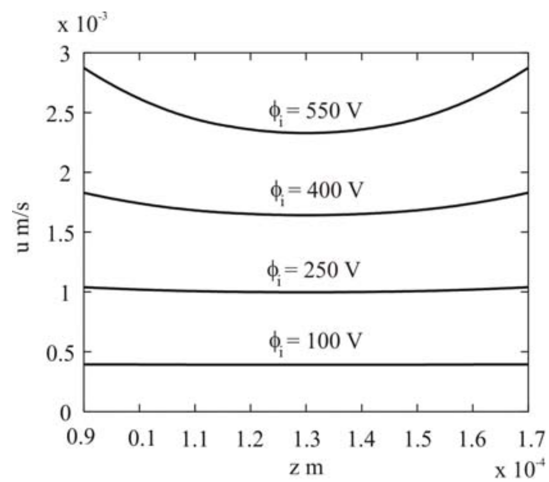

Figure 2: Liquid flow velocity distribution along the center line in the z-direction at the microchannel outlet (parameter: inlet applied electric potential)

Fig. 3 shows the curves for the time-dependent liquid temperature at the center point of the microchannel outlet, where the inlet applied electric potential is used as a parameter.

This figure also shows that the inlet applied electric potential has an influence on the liquid's temperature due to the Joule heating effect, which increases the liquid temperature when the applied electric potential rises.

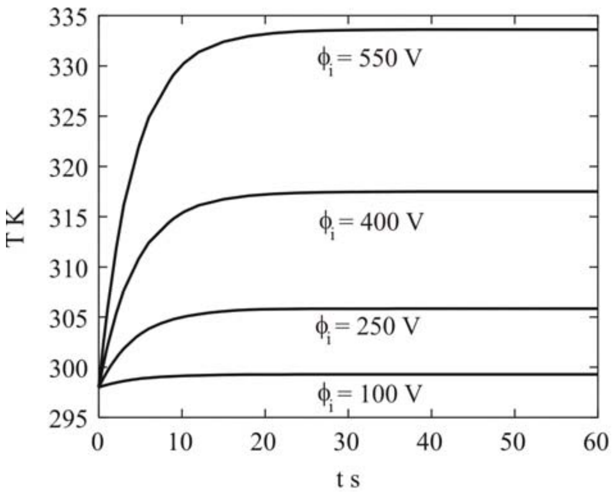

Figure 3: Liquid temperature versus time (parameter: inlet applied electric potential)

Fig. 4 shows the corresponding curves for liquid temperature as at the microchannel center line in x-direction at the time of 60 s, clearly showing that the liquid temperature rises as the distance from the microchannel increases.

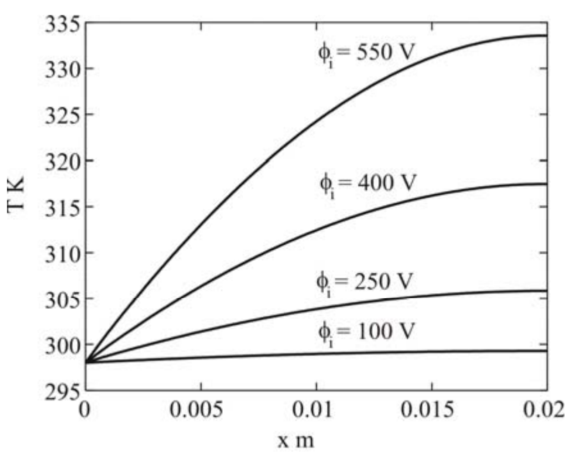

Figure 4: Liquid temperature distribution in the x-direction at the microchannel center line (parameter: inlet applied electric potential)

Joule Heating Effect on Liquid Flow Velocity and Temperature

To investigate the effect of the Joule heating on the liquid flow velocity and the liquid temperature, the inlet applied electric potential and the pressure difference were kept constant at 550 V and 0 kPa, respectively. The term $\sigma_L\left(\vec{E}.\vec{E}\right)$ in Eq. 8 was considered to account for the Joule heating effect and this term was neglected for the case without Joule heating. Fig. 5 shows the liquid flow velocity along the center line in the z-direction at the microchannel outlet, where it was found that with Joule heating the liquid flow velocity was higher than that without Joule heating. This can be explained by temperature-dependent thermophysical properties of the liquid. As shown in Fig. 6, Joule heating influence increases the liquid's temperature, and the Joule heating contribution also increases with applied electric potential.

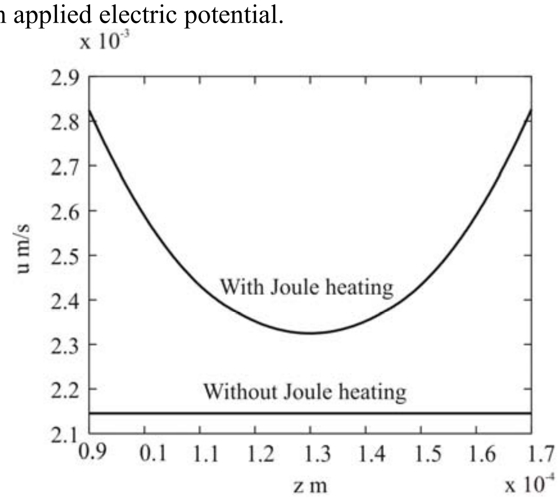

Figure 5: Liquid flow velocity distribution along the center line in the z-direction at the microchannel outlet (parameter: Joule heating)

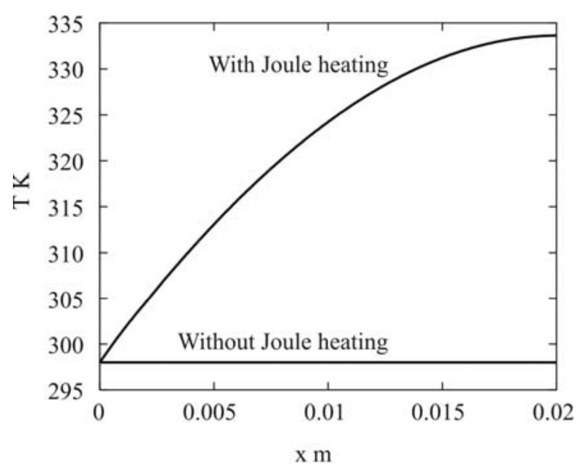

Figure 6: Liquid temperature distribution in the x-direction at the microchannel center line (parameter: inlet applied electric potential)

Effect of Pressure Difference on Liquid Flow Velocity and Temperature Distribution

To analyze the effect of pressure difference on liquid flow velocity, the heat transfer coefficient and the inlet applied electric potential were kept constant, at 10 $Wm^{-2}K^{-1}$ and 550 V, respectively. Pressure differences of 0 kPa, 5 kPa and 10 kPa were then selected. Fig. 7 shows the x-component liquid flow velocity along the center line in the z-direction at the microchannel outlet, where it was found that the liquid flow velocity increased in accordance with the increase in the pressure difference between the microchannel inlet and outlet. This was due to a larger volumetric flow rate induced as a result of the increased pressure difference between the microchannel inlet and outlet. For a fixed microchannel cross-section this led to a higher velocity, and the 0 kPa case corresponds to the pure electroosmotic flow.

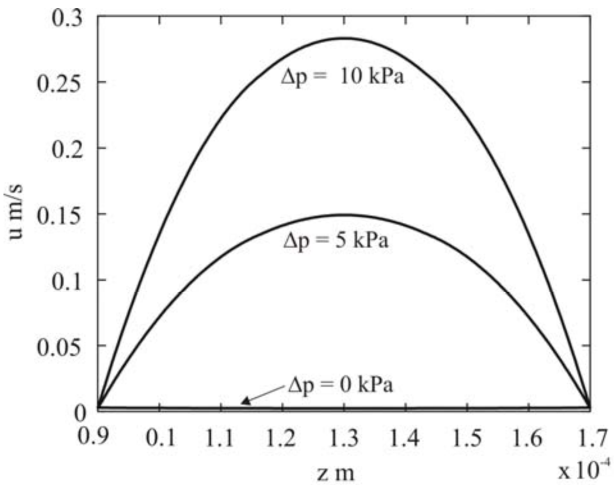

Figure 7: Liquid flow velocity distribution along the center line in the z-direction at the microchannel outlet (parameters: pressure difference)

Moreover, Fig. 8 shows the liquid temperature at the center point of the microchannel outlet as a function of time, thus showing that the steady-state value of the liquid temperature decreased according to the increasing pressure difference between the microchannel inlet and outlet. This was due to the decrease of the x-component liquid flow velocity in relation to the pressure difference decrease for the same imposed bottom wall heat transfer coefficient. In other words, the highest liquid temperature corresponds to the pure electroosmotic flow due to the lowest achieved liquid velocity in a microchannel, as Fig. 7 clearly shows.

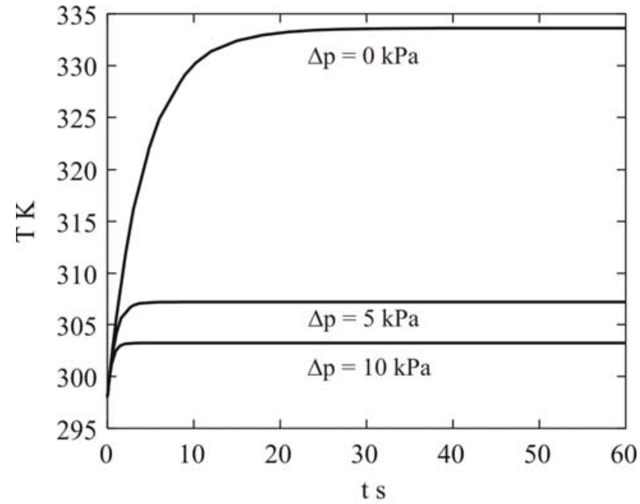

Figure 8: Temperature versus time (Parameter : pressure difference)

Effect of Heat Transfer Coefficient on Liquid Flow Velocity and Temperature Distribution

Two different heat transfer coefficient values of 10 $Wm^{-2}K^{-1}$ and 60 $Wm^{-2}K^{-1}$ were considered in order to analyze their effect on liquid flow velocity and liquid temperature distribution. Pressure difference and inlet applied electric potential were kept constant, using the values 0 kPa and 400 V, respectively. Temperature variation as a function of time, as shown in Fig. 9. It can also be observed that the time-dependent temperature at the center point of the microchannel outlet increases according to the increasing heat transfer coefficient on the bottom wall, which increases the heat flux on the bottom wall. Moreover, Fig. 10 shows the increasing steady-state liquid temperature in the x-direction at the center line of the microchannel, according to an increase in the heat transfer coefficient.

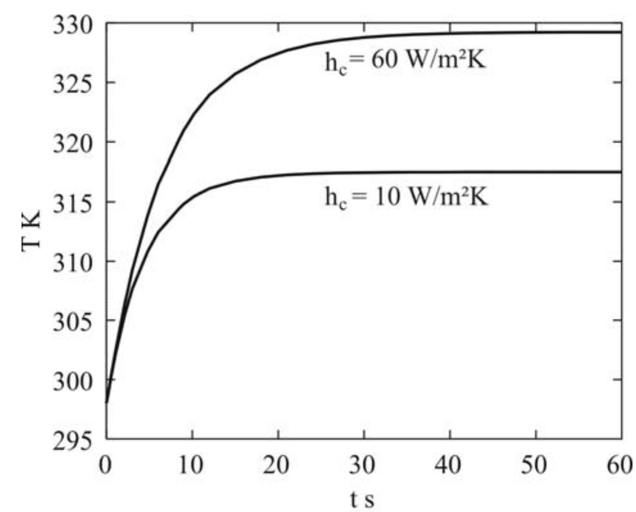

Figure 9: Temperature versus time (parameter : heat transfer coefficient)

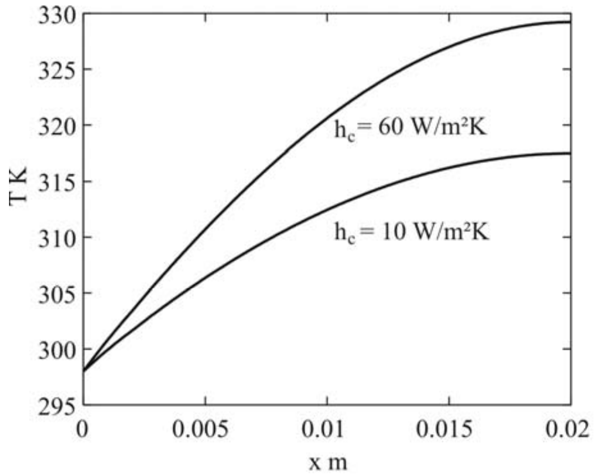

Figure 10: Liquid temperature distribution in the x-direction at the microchannel center line (parameter: heat transfer coefficient)

Given that liquid thermophysical properties are temperature-dependent, Fig. 11 shows there are variations in x-component liquid flow velocity along the center line in the z-direction at the microchannel outlet, when the heat transfer coefficient is used as a parameter. This clearly demonstrates that as liquid flow velocity increases, so too does the heat transfer coefficient. In other words, the liquid flow is accelerated, increasing the bottom wall heat flux due to the higher heat transfer coefficient.

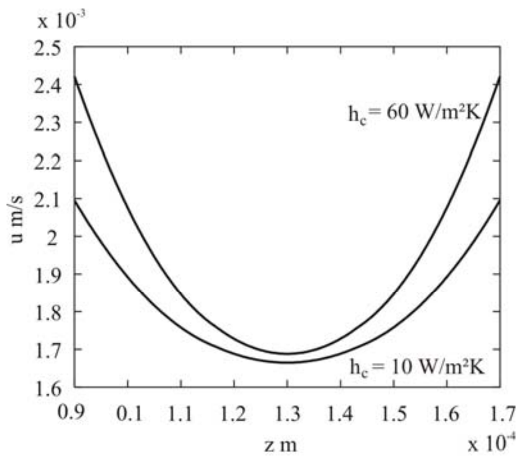

Figure 11: Liquid flow velocity distribution along the center line in the z direction at the microchannel outlet (parameter: heat transfer coefficient)

Effect of Microchannel Thickness on Temperature Distribution

To investigate the effect of the microchannel thickness on liquid flow and thermal characteristics, liquid cross-section height, inlet applied electric potential, the pressure difference and the heat transfer coefficient on microchannel bottom wall were kept constant, using the values 80 x 10^{-6} m, 400 V, 0 kPa and 10 $Wm^{-2}K^{-1}$, respectively. The thicknesses of 60 x 10^{-6} m, 90 x 10^{-6} m and 120 x 10^{-6} m were selected in order to analyze their effect on liquid flow velocity and liquid temperature distribution. Fig. 12 shows the steady-state liquid temperature distribution along the microchannel center line in the x direction, showing that the liquid temperature increases with increasing distance in the x direction. However this liquid temperature decreases when the microchannel thickness increases while keeping the liquid cross-section.

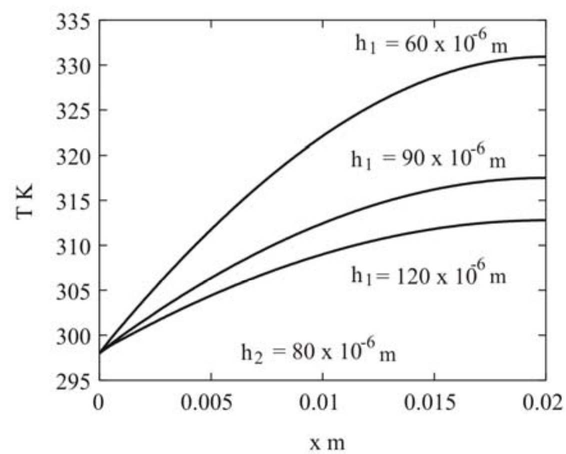

Figure 12: Liquid temperature distribution in the x-direction at the microchannel center line (parameter: micorchannel thickness)

Effect of Liquid Square Cross-Section Height on Temperature Field

To analyze the effect of the liquid square cross-section height on thermal characteristics, microchannel thickness, inlet applied electric potential, the pressure difference and the heat transfer coefficient were kept constant by using the values of 90 x 10^{-6} m, 400 V, 0 kPa and 10 $Wm^{-2}K^{-1}$, respectively. For this investigation the values 80 x 10^{-6} m, 95 x 10^{-6} m and 110 x 10^{-6} m were selected for the liquid square cross-section height . Fig. 13 shows the steady-state liquid temperature distribution along the microchannel center line in the x-direction. There, it is clearly observed that the liquid temperature increases according to the increasing height of liquid square crosssection, because the heat transfer surface increases with the increasing liquid square cross-section, keeping all other parameters unchanged.

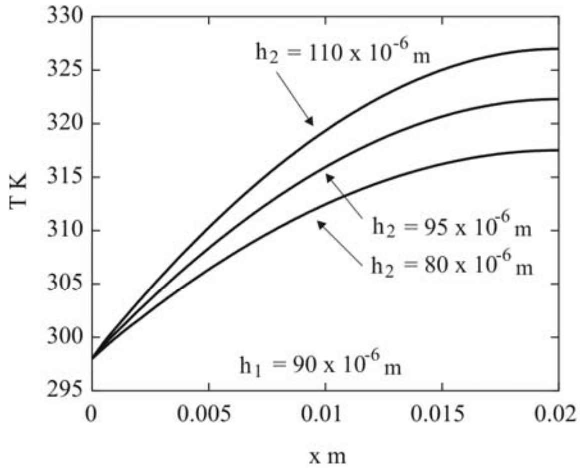

Figure 13: Liquid temperature distribution in the x-direction at the microchannel center line (parameter: liquid cross-section height)

Comparison of Results

The results found for the liquid flow velocity distribution when taking into account variations in the liquid thermophysical properties were compared with those obtained using the constant liquid thermophysical properties as shown in Fig. 14. This demonstrates that when considering the liquid constant thermophysical properties the steady-state electroosmotic liquid flow velocity is less than that reached for the liquid temperature-dependent thermophysical property case.

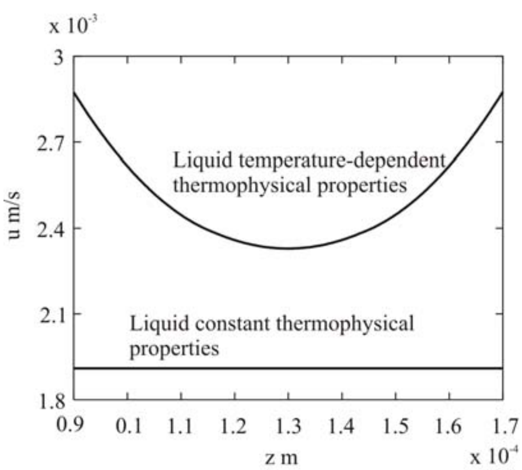

Figure 14: Liquid flow velocity distribution along the microchannel center line in the z-direction at the microchannel outlet (parameter: liquid properties)

CONCLUSION

In this study, transient laminar liquid flow and thermal characteristics in the three-dimensional microchannel of a square cross-section were numerically investigated using a computational dynamic code. The model developed accounted for electroosmotic and pressure-driven flow, heat transfer coefficient on the microchannel bottom wall, liquid temperature-dependent thermophysical properties and substrate properties. The results obtained demonstrate that variations in applied electric potential, pressure difference, heat transfer coefficients and in microchannel dimensions significantly affect liquid flow and thermal behavior in a microchannel, but in different ways. Finally, the results found were compared with those obtained for the liquid constant thermal properties.

ACKNOWLEDGMENTS

The authors are grateful to Foundation of University of Quebec in Abitibi-Temiscamingue (FUQAT).

REFERENCES

[1] N.-T. Nguyen, S. T. Wereley, Fundamentals and Applications of Microfluidics, second edition. Boston, London: Artech House Publishers, 2006.
[2] G. S. Kandlikar, S. Garimella, D. Li, S. Colin, M. R. King, Heat transfer and fluid flow in minichannels. Oxford, UK: Elsevier, 2006.
[3] Z. Li, W. Q. Tao, Y. L. He, A numerical study of laminar convective heat transfer in microchannel with non-circular cross-section, Int. Journal of Thermal Sciences 45, 2006, 1140–1148.
[4] P. van Male, M.H.J.M. de Croon, R.M. Tiggelaar, A. van den Berg, J.C. Schouten, Heat and mass transfer in a square microchannel with asymmetric heating.International Journal of Heat and Mass Transfer 47 (2004) 87–99.
[5]C. Wang, T. N. Wong, C. Yang, K. T, Ooi, Characterization of electroosmotic flow in rectangular microchannels. International Journal of Heat and Mass Transfer 50 (2007) 3115–3121.
[6] M. C. Yang, T. N.Wong, K. T. Ooi, Dynamic aspects of electroosmotic flow in rectangular microchannels. Int. Journal of Engineering Science, 42, 2004, 1459-1481.
[7] J. Yang, A. Bhattacharyya, J.H. Masliyah,c and D.Y. Kwok, Oscillating laminar electrokinetic flow in infinitely extended rectangular microchannels, Journal of Colloid and Interface Science, 261, 2003, 21–31.
[8] T. Zhou, A.-L. Liu, F.-Y. He, X.-H. Xia, Time-dependent starting profile of velocity upon application of external electrical potential in electroosmotic driven microchannels, Colloids and Surfaces A: Physicochem. Eng. Aspects 277, 2006, 136–144.

[9] COMSOL INC., COMSOL Multiphisics 3.5, user's guide and reference guide. Burlington, USA: COMSOL, 2008.
[10] F.P. Incropera, D.P. DeWitt, T.L. Bergman and A.S. Lavine, Fundamentals of Heat and Mass Transfer, sixth edition, Wiley, 2007.